Materials Science and Engineering C 31 (2011) 423–427

Contents lists available at ScienceDirect

Materials Science and Engineering C

journal homepage: www.elsevier.com/locate/msec

Fabrication, properties, and cytocompatibility of ZrC film on electropolished NiTi shape memory alloy

C.L. Chu [a,*], H.L. Ji [a], L.H. Yin [b], Y.P. Pu [b], P.H. Lin [a], Paul K. Chu [c]

[a] School of Materials Science and Engineering and Jiangsu Key Laboratory for Advanced Metallic Materials, Southeast University, Nanjing, 211189, China
[b] School of Public Health, Southeast University, Nanjing 210096, China
[c] Department of Physics and Materials Science, City University of Hong Kong, Hong Kong, China

ARTICLE INFO

Article history:
Received 25 February 2010
Received in revised form 29 September 2010
Accepted 29 October 2010
Available online 4 December 2010

Keywords:
NiTi shape memory alloy
ZrC film
Mechanical properties
Cytocompatibility

ABSTRACT

The microstructural characteristics, mechanical properties, and cytocompatibility of ZrC films deposited on electropolished NiTi shape memory alloy (SMA) by magnetron sputtering are investigated by scanning electron microscopy (SEM), X-ray photoelectron spectroscopy (XPS), X-ray diffraction (XRD), nanoindentation, and MTT test. The deposition rate of the ZrC film is smaller than the pure Zr film. Although ZrC is the only phase in the film, the pure ZrC film with small oxygen content is non-stoichiometric. The hardness and modulus increase initially with larger nanoindentation depths, reach maximum values, and then gradually decrease afterwards as a result of the composite effects of the ZrC film and NiTi substrate. Deposition of the ZrC film promotes proliferation of fibroblasts revealing enhanced cytocompatibility compared to uncoated NiTi.

1. Introduction

ZrC is an advanced ceramic due to superior covalent properties such as higher melting point compared to TiN, TaN and ZrN, great hardness, excellent mechanical stability, as lower work function as well as favorable metallic behavior such as electrical and optical properties [1,2]. Therefore, ZrC films are widely used in traditional hard and wear resistant coatings as well as emerging applications as nuclear fuel particle coatings, field emitter coatings, and thermophotovoltaic radiator coatings [3]. Moreover, Zr and C are biocompatible elements that can alter the surface chemistry for faster osteointegration and so ZrC has been used in multifunctional biocompatible films on biomedical implants [4,5]. Deposition of a ZrC film can improve the biological safety of biomedical NiTi shape memory alloys (SMA) [6–8] because the ZrC film as a barrier layer can minimize leaching of toxic nickel ions from the NiTi substrate and subsequent harmful and allergic effects. In fact, the release of nickel and its associated toxicity, carcinogenicity and allergic hazards have been well documented [9,10]. The effective solutions seem to depend on the improvement of surface microstructure and properties of this alloy. As a result, many surface modification methods have been considered and good progress has been made [11].

Based on our knowledge, there have been no systematic studies on the microstructural, mechanical, and biomedical characteristics of ZrC films deposited on NiTi SMA. In the work reported here, ZrC films are deposited on electropolished NiTi SMA by magnetron sputtering and the microstructure is studied by scanning electron microscopy (SEM), X-ray photoelectron spectroscopy (XPS), and X-ray diffraction (XRD). Furthermore, the mechanical properties and cytocompatibility are investigated by nanoindentation and MTT test.

2. Experimental details

2.1. Sample preparation

A commercially available NiTi (50.8 at.% Ni) SMA plate for medical applications with a martensite initiation temperature (M_s) of −12.8 °C and austenite finish temperature (A_f) of 33.4 °C were cut into small rectangular blocks with dimensions of 10 mm × 10 mm × 1 mm. The samples were chemically polished for several minutes using a solution containing H_2O, HF (40 wt.%), HNO_3(65 wt.%) with a volume ratio of 5:1:4 and then electropolished at a constant voltage of 10 V for 6 min at room temperature in an electrolytic cell with a magnetic stirrer and graphite cathode. The electrolyte consisted of 21 vol.% perchloric acid ($HClO_4$, 70–72%) and 79 vol.% acetic acid (CH_3COOH, 99.5%). Afterwards, the samples were ultrasonically cleaned successively in acetone and deionized water for 10 min each before being divided into two groups with the first group being the control.

The second group of samples was deposited with ZrC films using a reactive DC magnetron sputtering system (JGP450A2, Shenyang Zky Technology Development Co. Ltd, China). A system pressure of 1×10^{-3} Pa was attained prior to film deposition and the carrier gas (Ar) had a purity of 99.95%. The substrates were firstly cleaned by

* Corresponding author.
E-mail address: clchu@seu.edu.cn (C.L. Chu).

0928-4931/$ – see front matter © 2010 Elsevier B.V. All rights reserved.
doi:10.1016/j.msec.2010.10.023

argon sputtering for 6 min and during deposition, the working pressure was fixed at 0.5 Pa and the total flux was 30 cm^3/min. The NiTi substrate was heated to only 250 °C during deposition because it is well known that significant aging and degradation of the shape memory effect occur in NiTi SMA at temperature over 300 °C [6,12]. During deposition, the DC power was about 150 W which was equivalent to a target DC offset voltage of 400 V and the substrate current was 0.36 A for a substrate bias of −50 V. The distance between the target and substrate holder was 60 mm. A Zr-C composite target with a 1 to 1 area ratio of Zr (99.9%) to C (99.9%) was used and the target was 80 mm in diameter and 3 mm thick. The deposition time was about 60 min.

2.2. Microstructural characterization

The surface and cross section morphologies were evaluated by field-emission scanning electron microscopy (SEM, Sirion 2000, FEI Co.) at 20 kV after the surfaces were coated with gold. X-ray diffraction (RAD IIA, Rigaku, Japan) with a Cu K_α source operated at 40 kV and 25 mA was used to determine the phase composition.

The samples were analyzed by XPS using a VG Scientific ESCALAB 5 spectrometer with a monochromatic Al K_α (1486.6 eV) X-ray source. The base pressure in the analysis chamber was better than 10^{-8} mbar. Survey spectra in the range 0–1400 eV were recorded for each sample at 50 eV constant pass energy and high-resolution spectra of Zr3d, C 1 s and O 1 s ranges using a 20 eV pass energy were also acquired. The high-resolution XPS spectra were used to determine the chemical states as well as concentrations.

2.3. Nanoindentation

The mechanical properties and deformation behavior were investigated by nanoindentation using a nanoindenter (MTS Nano Instruments XP) equipped with the continuous stiffness measurement (CSM) capability and the indentation was carried out using a Berkovich (three-sided pyramid) indenter. A small-harmonic, high-frequency amplitude was superimposed over the indentation loading and the contact stiffness of the sample was measured from the displacement response at the excitation frequency. The nanoindentation experiment was conducted in displacement control to a depth of 2000 nm, which can result in a relatively large-area three-sided pyramid indentation with the edge length above 12 μm on each sample [13]. The modulus and hardness values were derived instantaneously as a function of depth from the contact stiffness. The load and hardness calibration were performed employing a fused silica reference. At least three indentations were conducted on each sample to obtain averages.

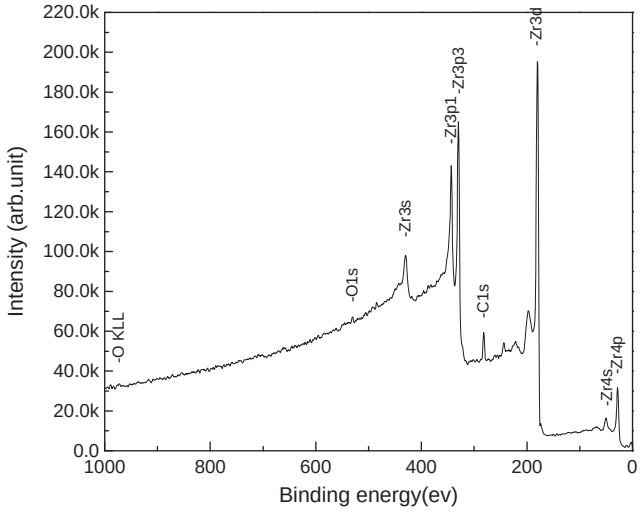

Fig. 2. XPS survey spectra of the ZrC film surface.

2.4. MTT test

In the MTT test, fibroblasts L929 were cultured in Dulbecco's minimal essential media (DMEM) supplemented with 15% (v/v) fetal calf serum at 37 °C in an atmosphere of 5% CO_2 and 95% air. The cleaned samples were fixed onto the bottom of a 24-well tissue culture plate. One ml of the cell suspension consisting of 1×10^5 cells was then seeded onto the surface of each sample and the wells without any sample served as the control in the MTT (3-[4, 5-dimethylthiazol-2-yl]-2, 5-diphenytetrazolium bromide) cytotoxicity test. The 24-well plates were incubated at 37 °C under an atmosphere of 5% CO_2 and 95% air. After culturing for 24 h, the medium in the wells was replaced with 100 μl of 0.5% MTT and 400 μl DMEM and the samples were incubated at 37 °C under an atmosphere of 5% CO_2 and 95% air for 4 h. Afterwards, the cells were dissolved by dimethylsulfoxide (DMSO) and agitated for 10 min. The optical absorbance of the fluid was monitored at a wavelength of 575 nm (620 nm reference). The relative growth rate (*RGR*) of the fibroblasts on the surface of the sample was calculated according to the following formula:

$$RGR = \frac{D_t}{D_n}\frac{A_n}{A_t} \times 100\%, \quad (1)$$

where D_t, D_n, A_t and A_n are the absorbencies of the sample and the negative control group as well as areas of the sample and the well of 24-well tissue culture plate for the negative control, respectively.

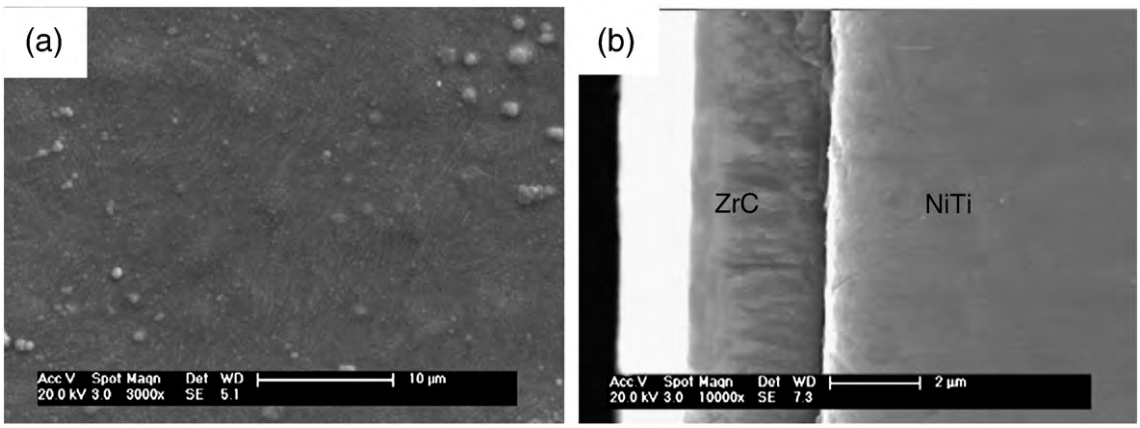

Fig. 1. SEM images of ZrC film: (a) Surface morphology and (b) Cross section.

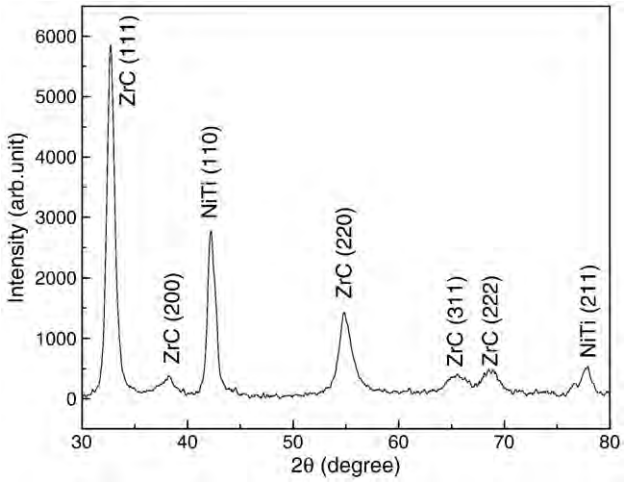

Fig. 3. XRD patterns obtained from the ZrC film deposited on NiTi.

The experimental results were expressed as mean values ± standard deviation. The Student's *t*-test was used for statistical analysis.

3. Results and discussions

3.1. Fabrication and microstructure

The ZrC film deposited on the NiTi shown in Fig. 1(a) has a dense surface structure and some surface particles composed of Zr and C as determined by energy-dispersive X-ray analysis (EDS). The cross sectional morphologies in Fig. 1(b) indicate the ZrC film is about 2.5 μm thick and adheres well to the NiTi substrate.

It should be pointed out that under similar conditions, the thickness of the ZrC film is only about half of that of pure Zr film as reported previously [14]. There are two reasons. First of all, the Zr-C composite target is composed of pure Zr (99.9%) and pure graphite (99.9%) with an area ratio of 1:1 and can provide enough active C atoms for the chemical reaction. A thin ZrC compound film formed on the target surface may reduce the target sputtering rate and subsequently deposition efficiency. The latter phenomenon is called "target poisoning" [15]. Secondly, under a certain power, the sputtering yield of C spattering is only about 1/3 of that of Zr [15], and the area of exposed Zr metal is only about half of the target.

Fig. 2 shows the typical XPS survey spectrum disclosing that the dominant surface elements are Zr and C. The amounts of Zr, C, and O are about 66.6 at.%, 26.5 at.%, and 6.9 at.%, respectively. The calculated Zr/C atomic ratio is about 2.5, which is not consistent with the ratio of Zr to C spattering yields. It is apparently affected by carbon contamination in the quantitative analysis.

Fig. 3 depicts the XRD pattern of the ZrC film on NiTi and the desired ZrC compound is the predominant phase in the film. With the exception of the (110) and (211) peaks corresponding to the intermetallic NiTi substrate phase, there are no other peaks associated with the Zr or ZrO_2 phase. That is, the ZrC film is non-stoichiometric.

Absorption of oxygen leading to the existence of oxygen in ZrC film is consistent with the high affinity between Zr for O [16]. In general, ZrC synthesized at low temperature contain high oxygen contents. However, the O content measured from our ZrC film here is less than 10 at.%. It is believed to be due to the characteristics of magnetron sputtering. During the formation of ZrC film by magnetron sputtering, heating in vacuum can lead to the following reaction between zirconium oxide (ZrO_2) and C [17,18]:

$$3C + ZrO_2 = ZrC + 2CO\uparrow \quad (2)$$

$$ZrO_2 + C = ZrC + 2O \text{ (absorb)}. \quad (3)$$

It is clear that the zirconium carbide forms simultaneously with the oxidized zirconium overlayer decomposition. And partial oxygen was absorbed by the ZrC film. Thus, it is reasonable that O can be detected by XPS but ZrO_2 is not present in XRD pattern.

The Zr3d and C1s XPS spectra acquired from the surface of ZrC film are shown in Fig. 4. The Zr3d spectrum can be deconvoluted into two peaks as shown in Fig. 4(a). The two different peaks correspond to the ZrC compound with a doublet consisting of $Zr3d_{5/2}$ (179.1 eV) and $Zr3d_{3/2}$ (181.5 eV) [16]. Fig. 4b indicates that the dominant peak is at 282.1 eV which can be assigned to C1s of the carbide (ZrC).

3.2. Mechanical properties

Fig. 5a shows the representative load vs. displacement curves acquired from different samples by nanoindentation in an effort to determine the mechanical characteristics [19]. The needed load increases with depths from the surface. At the same nanoindentation depth, the load of the ZrC film is higher than that of the electropolished NiTi SMA, indicating that the deposited ZrC film can enhance the load bearing ability of NiTi.

Fig. 5b and c shows the corresponding hardness and Young's modulus values, respectively obtained from the CSM system. The hardness and modulus determined from each sample display a similar

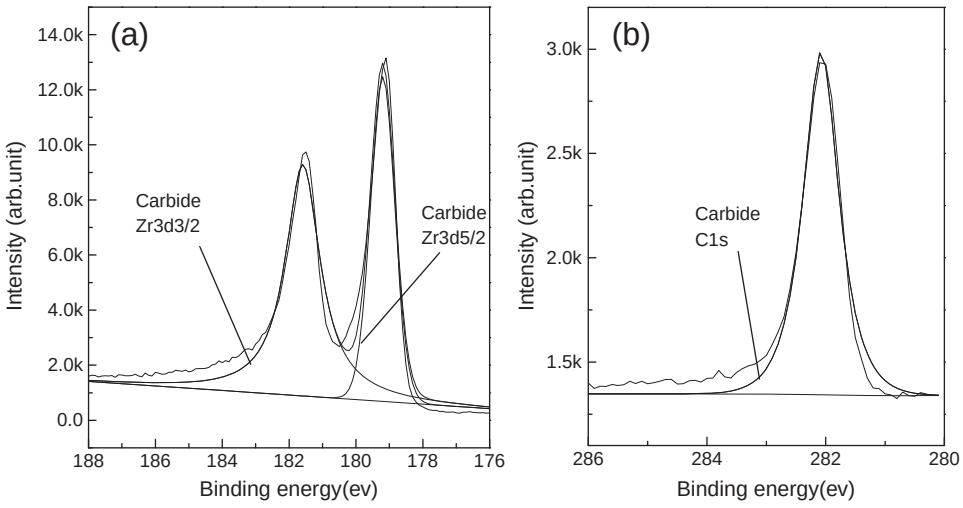

Fig. 4. (a) Zr3d and (b) C1s XPS spectra acquired from the ZrC film.

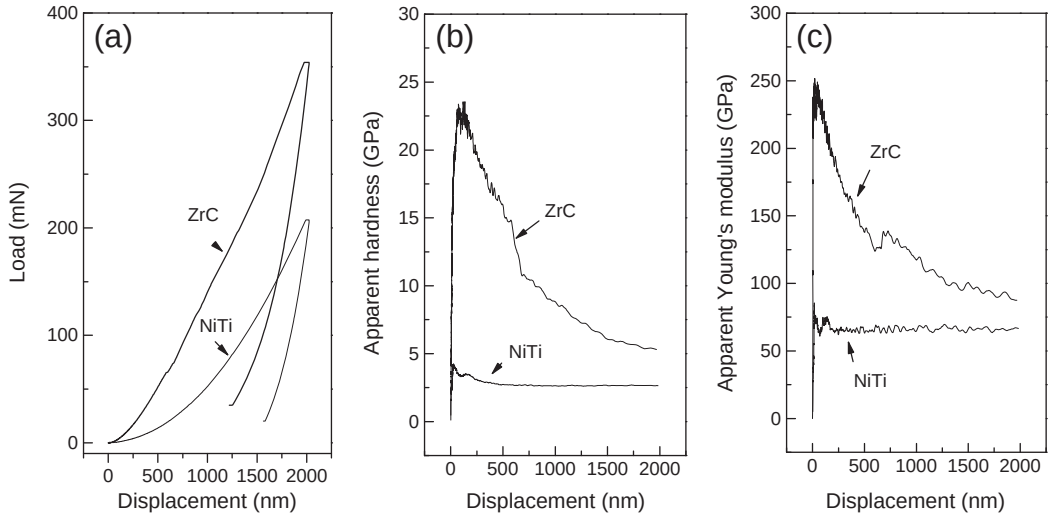

Fig. 5. Surface mechanical characteristics: (a) Load, (b) Apparent hardness, and (c) Apparent Young's modulus vs. nanoindentation displacement (depth) of EP-NiTi SMA (NiTi) and ZrC film (ZrC).

trend with increasing depths. The hardness and modulus values not only depend on the surface films, but also are influenced by the NiTi substrate because the total nanoindentation depth of 2000 nm is larger than or comparable to the thickness of the surface films. The native titania film on the electropolished NiTi SMA control is about 10 nm thick, whereas the ZrC film is about 2500 nm thick.

At the initial stage of nanoindentation, the hardness and modulus values of the electropolished NiTi SMA reach their maximum values, 4.2 GPa and 85 GPa, respectively. This is because the thickness of the native titania film on the electropolished NiTi sample is generally less than 10 nm and contributions from the NiTi substrate that can decrease the hardness and modulus values arise earlier. With increasing depths, the hardness and modulus values decrease finally reaching a plateau near 2.7 GPa and 66 GPa, respectively, resulting from the composite hardness and modulus encompassing the hardness and modulus values of the titania film and NiTi substrate.

The hardness and modulus values obtained from the ZrC film on NiTi first increase with larger nanoindentation depths due to increased densification of the ZrC film and then reach their maximum values of about 24 GPa and 250 GPa, respectively. Afterwards, they gradually decrease when the indentation depth is comparable to the thickness of ZrC film. That is, the indentation front is gradually approaching the substrate surface. Thus, the variations in the hardness and modulus values in this region result from the increasing contributions from the NiTi substrate that can decrease the modulus values. Actually, the nanoindentation response of NiTi alloys is characterized by complex mechanisms. Kumar et al. examined the effects of TiN protective coatings on phase transformation behavior and nanoindentation properties of NiTi films [20,21]. It is found that TiN/NiTi films were observed to show larger hysteresis compared to pure NiTi films, which could be due to phase transformation and additional strain in NiTi films because of top TiN layer. Thus, the interactions between ZrC film and NiTi substrate do exist and still need further research in subsequence.

The composite modulus and composite hardness values derived from the ZrC film and NiTi substrate are higher than those of the electropolished NiTi SMA. The desirable properties can be attributed to the inherent properties of ZrC. It is common to determine the average intrinsic properties of the thin film at indentation depths of less than 10% of the film thickness in order to minimize contributions from the substrate [22]. In this work, the measured average intrinsic hardness and modulus of the ZrC film are about 19.1 GPa and 228.9 GPa, respectively, which are consistent with those reported previously [1].

Table 1
Results of MTT tests performed on the EP-NiTi SMA and ZrC-NiTi.

Materials	Culture time	Optical density	Relative growth rates (RGR) (%)
EP-NiTi SMA	1 day	0.425 ± 0.047	139
	3 days	0.803 ± 0.089	167
	7 days	0.979 ± 0.119	154
ZrC	1 day	0.555 ± 0.061	182
	3 days	1.007 ± 0.111	210
	7 days	1.338 ± 0.147	210
Negative control	1 day	0.640 ± 0.071	100
	3 days	1.009 ± 0.111	100
	7 days	1.336 ± 0.147	100

3.3. Cytocompatibility

The MTT reagent is a pale yellow substance that is reduced to a dark blue formazan product when incubated with viable cells. Therefore, the production of formazan can reflect the level of cell viability. The cells observed in the vicinity of the two samples after co-culturing with fibroblasts L929 exhibit the normal morphology and attach to the sample surfaces. These results suggest that the samples are well tolerated by the fibroblasts. Table 1 shows the results of MTT tests. The cells cultured on the ZrC film show a higher RGR value than those on the electropolished NiTi SMA. Hence, it can be inferred that ZrC film promotes proliferation of the fibroblasts.

4. Conclusions

ZrC films are deposited on electropolished NiTi shape memory alloy samples by magnetron sputtering to enhance the surface mechanical properties and cytocompatibility. ZrC is the only phase detected from the film although it is non-stoichiometric. The ZrC film has a lower than expected oxygen content due to the characteristics of magnetron sputtering. The hardness and modulus values determined from the ZrC film on NiTi increase initially with larger nanoindentation depths, reach maximum values, and diminish gradually resulting from the composite hardness and modulus of the ZrC film and NiTi substrate. The cell viability test reveals better proliferation of fibroblasts on the ZrC, suggesting better cytocompatibility on the ZrC/NiTi system compared to electropolished NiTi.

Acknowledgements

The work was supported by Program for New Century Excellent Talents (NCET-06-0464) in University of Ministry of Education of China, Natural Science Foundation of Jiangsu Province (Project No.: BK2007515), and City University of Hong Kong Strategic Research Grant (SRG) No. 7008009.

References

[1] C.S. Chen, C.P. Liu, C.Y.A. Tsao, Thin Solid Films 479 (2005) 130.
[2] Y.S. Won, V.G. Varanasi, O. Kryliouk, T.J. Anderson, L. McElwee-White, R.J. Perez, Journal of Crystal Growth 307 (2007) 302.
[3] D. Craciun, G. Socol, N. Stefan, G. Bourne, V. Craciun, Applied Surface Science 255 (2009) 5260.
[4] D.V. Shtansky, N.A. Gloushankova, I.A. Bashkova, M.I. Petrzhik, A.N. Sheveiko, F.V. Kiryukhantsev-Korneev, I.V. Reshetov, A.S. Grigoryan, E.A. Levashov, Surface & Coatings Technology 201 (2006) 4111.
[5] Y.F. Zheng, X.L. Liu, H.F. Zhang, Surface & Coatings Technology 202 (2008) 3011.
[6] K. Otsuka, C.M. Wayman, Shape Memory Materials, Cambridge University Press, Cambridge, 1998.
[7] L. Yahia, Shape Memory Implants, Springer, Berlin, 2000.
[8] T. Duerig, A. Pelton, D. Stockel, Materials Science and Engineering A273–275 (1999) 149.
[9] WilliamsD.F. , Toxicology of implanted metals. Fundamental aspects of biocompatibility, CRC Series in Biocompatibility, Vol II, CRC Press, Boca Raton, FL, 1981, p. 45.
[10] K. Takamura, K. Hayashi, N. Ishinishi, T. Yamada, Y. Sugioka, Journal of Biomedical Materials Research 28 (1994) 583.
[11] X.Y. Liu, P.K. Chu, C.X. Ding, Materials Science and Engineering R 47 (2004) 49.
[12] Y.N. Liu, X. Chen, P.G. McCormick, Journal of Materials Science 32 (1997) 5979.
[13] G.A. Crawford, Acta Biomaterialia 3 (3) (2007) 359.
[14] H.L. Ji, C.L. Chu, R.M. Wang, X.H. Zhang, W.Y. Zhang, Y.S. Dong, C. Guo, X.B. Sheng, P.H. Lin, P.K. Chu, Rare Metal Materials and Engineering 38 (2) (2009) 295.
[15] W.Z. Tan, Preparation Principle, Technology and Applications of Thin Films, 2nd ed. Metallurgy industry Press, Beijing, 2003.
[16] M. Matsuoka, S. Isotani, W. Sucasaire, N. Kuratani, K. Ogata, Surface & Coatings Technology 202 (2008) 3129.
[17] Q.F. Tong, J.L. Shi, Y.Z. Song, X.F. Hu, L. Liu, Aerospace Materials & Technology 2 (2004) 45.
[18] D.L. Cocke, M.S. Owens, Applied Surface Science 31 (1988) 471.
[19] W.C. Oliver, G.M. Pharr, Journal of Materials Research 7 (1992) 1564.
[20] A. Kumar, D. Kaur, Surface & Coatings Technology 204 (2009) 1132.
[21] A. Kumara, D. Singh, R. Kumar, D. Kaur, Journal of Alloys and Compounds 479 (2009) 166.
[22] A.C. Fischer-Cripps, Nanoindentation, 2nd ed.Springer, New York, 2004.